Capsule Growth in *Cryptococcus neoformans* Is Coordinated with Cell Cycle Progression

Rocío García-Rodas,[a] Radames J. B. Cordero,[b] Nuria Trevijano-Contador,[a] Guilhem Janbon,[c] Frédérique Moyrand,[c] Arturo Casadevall,[d] Oscar Zaragoza[a]

Mycology Reference Laboratory, National Centre for Microbiology, Instituto de Salud Carlos III, Majadahonda, Madrid, Spain[a]; Department of Biochemistry, Federal University of Rio de Janeiro, Rio de Janeiro, Brazil[b]; Unité Biologie et Pathogénicité Fongiques, Institut Pasteur, Paris, France[c]; Department of Microbiology and Immunology, Albert Einstein College of Medicine, Bronx, New York, USA[d]

ABSTRACT **The fungal pathogen *Cryptococcus neoformans* has several virulence factors, among which the most important is a polysaccharide capsule. The size of the capsule is variable and can increase significantly during infection. In this work, we investigated the relationship between capsular enlargement and the cell cycle. Capsule growth occurred primarily during the G_1 phase. Real-time visualization of capsule growth demonstrated that this process occurred before the appearance of the bud and that capsule growth arrested during budding. Benomyl, which arrests the cells in G_2/M, inhibited capsule growth, while sirolimus (rapamycin) addition, which induces G_1 arrest, resulted in cells with larger capsule. Furthermore, we have characterized a mutant strain that lacks a putative G_1/S cyclin. This mutant showed an increased capacity to enlarge the capsule, both *in vivo* (using *Galleria mellonella* as the host model) and *in vitro*. In the absence of Cln1, there was a significant increase in the production of extracellular vesicles. Proteomic assays suggest that in the *cln1* mutant strain, there is an upregulation of the glyoxylate acid cycle. Besides, this cyclin mutant is avirulent at 37°C, which correlates with growth defects at this temperature in rich medium. In addition, the *cln1* mutant showed lower intracellular replication rates in murine macrophages. We conclude that cell cycle regulatory elements are involved in the modulation of the expression of the main virulence factor in *C. neoformans*.**

IMPORTANCE ***Cryptococcus neoformans* is a pathogenic fungus that has significant incidence worldwide. Its main virulence factor is a polysaccharide capsule that can increase in size during infection. In this work, we demonstrate that this process occurs in a specific phase of the cell cycle, in particular, in G_1. In agreement, mutants that have an abnormal longer G_1 phase show larger capsule sizes. We believe that our findings are relevant because they provide a link between capsule growth, cell cycle progression, and virulence in *C. neoformans* that reveals new aspects about the pathogenicity of this fungus. Moreover, our findings indicate that cell cycle elements could be used as antifungal targets in *C. neoformans* by affecting both the growth of the cells and the expression of the main virulence factor of this pathogenic yeast.**

Received 19 February 2014 **Accepted** 19 May 2014 **Published** 17 June 2014

Citation García-Rodas R, Cordero RJB, Trevijano-Contador N, Janbon G, Moyrand F, Casadevall A, Zaragoza O. 2014. Capsule growth in *Cryptococcus neoformans* is coordinated with cell cycle progression. mBio 5(3):e00945-14. doi:10.1128/mBio.00945-14.

Editor Joseph Heitman, Duke University

Address correspondence to Oscar Zaragoza, ozaragoza@isciii.es.

Cryptococcus neoformans is a facultative intracellular fungal pathogen that causes meningitis, primarily in immunocompromised patients (1, 2). Its incidence increased significantly in association with the HIV pandemic, and it is estimated to cause more than 650,000 deaths per year, mainly in developing areas (3).

The best-characterized virulence factors of *C. neoformans* are a polysaccharide capsule (reviewed in reference 4), melanin production (5, 6), and the ability to grow at body temperature (7). During infection, *C. neoformans* undergoes changes that contribute to its persistence. These changes include capsule enlargement and the appearance of titan/giant cells (8–10).

A characteristic feature of the capsule is its ability to enlarge in response to certain environmental conditions (11–16). This process is believed to be essential for yeast survival in the host, because capsule growth confers protection against host defense mechanisms, including oxidative stress (17). Moreover, capsule enlargement has been correlated with increased intracranial pressure during human cryptococcal meningitis (18). Although capsule enlargement is an early response of the pathogen during infection, little is known about its regulation and the underlying molecular mechanisms that regulate this process. Recent articles have highlighted the importance of some transcription factors (such as Ada2, Rim101, and Gat201) in this process (19–21), indicating that capsule growth occurs through the induction of a gene expression rearrangement. In addition, the structurally conserved Pbs2-Hog1 mitogen-activated protein (MAP) kinase cascade controls morphological differentiation and virulence factors in serotype A *C. neoformans* (22).

In this study, we investigated the hypothesis that capsule enlargement in *C. neoformans* is coordinated with the cell cycle. This idea was hypothesized from different pieces of evidence. Under conditions of capsule growth, there is normally a decrease in the growth rate of the yeast, which suggests that factors that elongate some phases of the cell cycle result in capsule enlargement. In

addition, we hypothesize that capsule enlargement occurs mainly in G_1, prior to the emergence of the bud, because the addition of more polysaccharide during the $S/G_2/M$ phases might interfere with budding and the subsequent separation of the bud from the mother cell. Furthermore, several findings from the literature indicate that there is a correlation between capsule size and cell body size (11, 23), and the fact that cell body growth occurs mainly in G_1 suggests capsule growth would occur in the same cell cycle phase.

Cell cycle control has been extensively studied in *Saccharomyces cerevisiae* (24, 25), *Schizosaccharomyces pombe* (26), and *Ustilago maydis* (27). Cell cycle progression depends on the activity of a cyclin-dependent kinase (Cdk1/Cdc28/Cdc2), which remains low during G_1 and increases its kinase activity during the rest of the phases (28). The transition between G_1 and S is regulated by specific G_1/S cyclins (29, 30). However, little is known about the cell cycle regulation in *C. neoformans*. This yeast replicates by budding, and during the exponential phase, budding and DNA synthesis occur simultaneously (31). However, at the end of the exponential phase, budding is delayed and cells are arrested at G_1 or G_2 phases (32, 33).

To test our hypothesis, we have investigated and modulated cell cycle progression during capsule growth. In addition, we have investigated capsular phenotypes in a *C. neoformans* mutant lacking a putative cyclin. Our results indicate that capsule growth is linked to cell cycle progression and, in particular, to the G_1 phase. Therefore, we conclude that the link between cell cycle elements and capsule growth reveals new aspects about the biology of this virulence factor.

RESULTS

Analysis of DNA content during capsule growth. We first investigated whether capsule growth changed during the cell cycle progression of *C. neoformans*. Consistent with our initial hypothesis, capsule enlargement occurred mainly during the G_1 phase, so we expected that the cells would arrest in this phase after transfer to capsule-inducing medium. As shown in Fig. 1A, cells grown overnight at 30°C in Sabouraud medium were mainly in the G_2 phase. However, when cells were transferred to capsule-inducing medium, we observed an arrest in G_1 (shown as "n" in Fig. 1A).

Capsule sizes were measured in parallel at the different time points to confirm capsule enlargement in the capsule-inducing medium. Capsule growth was already noticeable after 3 h of incubation under these conditions, and the process continued after 6 h ($P < 0.05$) (Fig. 1B).

Capsule enlargement process is altered in the presence of cell cycle inhibitors. We studied the effect of cell cycle inhibitors on capsule growth. We first used sirolimus (rapamycin), which is an inhibitor of the TOR pathway and produces G_1 arrest. Sirolimus promoted capsule enlargement of *C. neoformans* in capsule-inducing medium (Fig. 2A). For both concentrations tested (0.5 and 1 μg/ml), the capsule sizes were significantly larger in cells exposed to sirolimus relative to the control condition (capsule-inducing medium with dimethyl sulfoxide [DMSO]) ($P < 0.05$). To ensure that sirolimus was inhibiting cell cycle progression, we performed growth curve experiments under the same conditions and observed a significant defect in the growth rate at the concentrations used (Fig. 2B).

We also used benomyl, an inhibitor of microtubule polymerization that induces M-phase arrest. Benomyl inhibited capsule enlargement of *C. neoformans* under capsule-inducing conditions (Fig. 2C) ($P < 0.05$). In addition, benomyl inhibited yeast growth at both concentrations tested (Fig. 2D). To discard the possibility that inhibition of capsule growth was not a consequence of cell death induced by the drug, we measured the viability of the cells after benomyl treatment by propidium iodide (PI) staining. We found that approximately 80% of the cells were alive after incubation with benomyl at the highest concentration tested (data not shown), indicating that lack of capsule growth was not a consequence of cell death.

Capsule growth visualization by time-lapse microscopy. According to our hypothesis, capsule growth should stop or diminish during budding, so we used time-lapse microscopy to visualize capsule growth. The capsule, however, is not visible under regular conditions given its high water content and similar refractive properties to that of the medium. Different methods have been described to visualize the capsule by light microscopy, with India ink negative staining being the easiest and most widely used in the literature. We tried to induce capsule growth in medium containing India ink, but we observed that under these conditions, capsular enlargement was impaired (result not shown), suggesting that the India ink interferes with the process. Another way to visualize the capsule is based on a phenomenon known as the capsular "quellung" reaction (34–37), which involves a change in the capsule's optical properties (i.e., refraction index) following binding of specific monoclonal antibodies (MAbs) to the capsular polysaccharide. The resulting Ab-coated capsule can be readily visualized using Nomarski microscopy (also known as differential interference contrast [DIC]). Given that the IgM MAb 13F1 induced a capsular reaction without significantly affecting the mechanical properties of the capsule (38), this antibody was used to visualize capsule enlargement as a function of time (Fig. 3A). When cells were transferred to capsule-inducing medium, enlargements of the cell and capsule were observed at 3.6 and 8.8 nm/min, respectively (Fig. 3B; see Movie S1 in the supplemental material). When the capsule reached a certain size (approximately 6 μm), the cell cycle progressed with the subsequent appearance of the bud and a decrease in capsule growth (Fig. 3B). Interestingly, after budding, the mother cells with enlarged capsule underwent a new round of cell cycle with no further cell or capsule growth (see Movie S1).

Identification of G_1/S cyclins in *C. neoformans*. Next, we investigated capsular phenotypes in mutants affected in cell cycle regulation. For this purpose, we identified G_1/S cyclins in *C. neoformans* by looking for homologues of the corresponding *CLN1* gene from *Ustilago maydis* (39). Since this organism is also a basidiomycete, we reasoned that the *C. neoformans* cell cycle proteins were more homologous to this organism than to those from members of the ascomycetes, such as *Saccharomyces cerevisiae*, *Schizosaccharomyces pombe*, or *Candida albicans*. After performing a BLAST comparison using the Cln1p from *U. maydis* against the *C. neoformans* genome database available at the Broad Institute, we identified the open reading frame (ORF) CNAG_06092, which was already annotated as a putative cyclin gene. We obtained the corresponding mutant from a library of targeted disruptants available at the ATCC (20).

We reconstituted the wild-type (wt) gene in this mutant. For this purpose, the wild-type gene was fused to the Neo marker, which confers resistance to Geneticin, using fusion PCR (see Materials and Methods). The DNA construct was integrated into the genome by biolistic transformation. In this way, we continued this

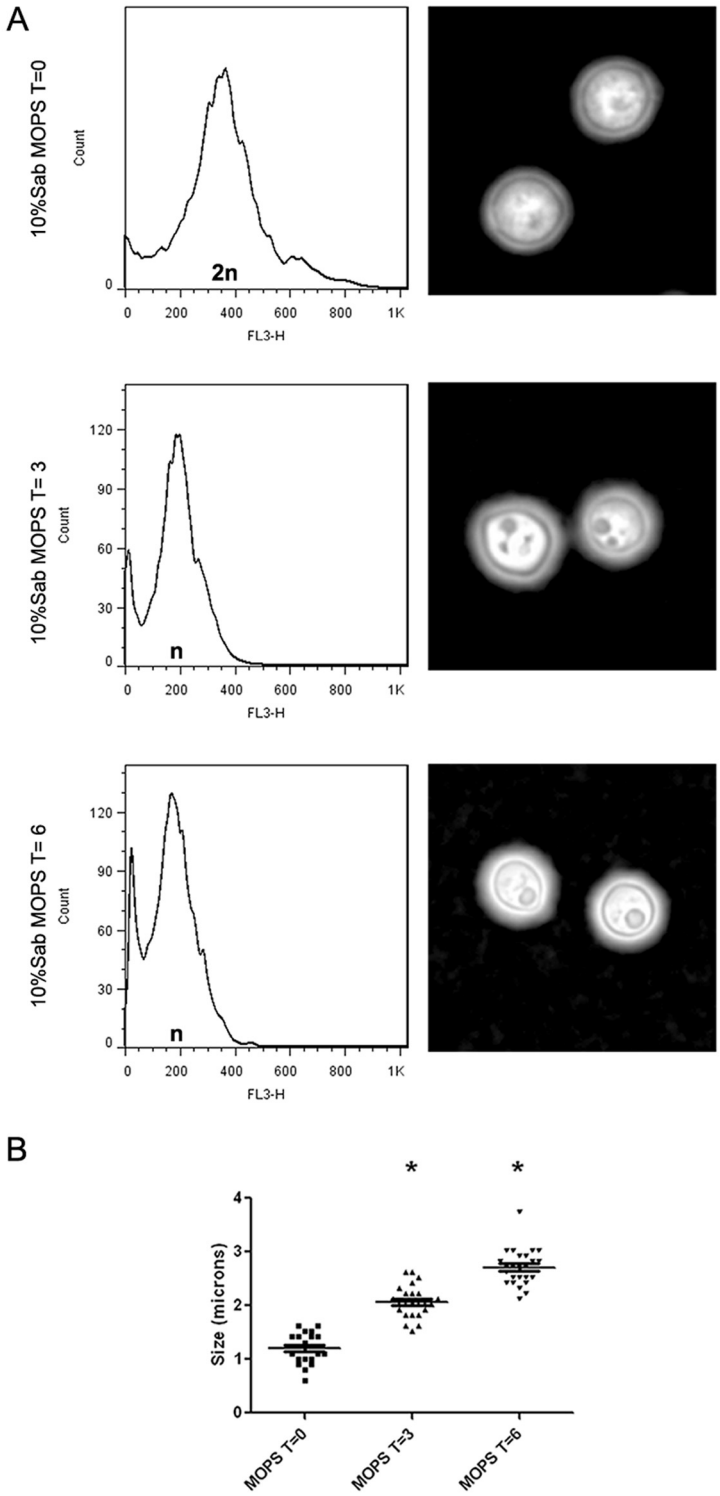

FIG 1 Flow cytometry analysis of cell cycle progression during capsule enlargement. (A) Samples were taken for flow cytometry analysis at the time indicated after PI staining (see Materials and Methods). Micrographs of cells suspended in India ink were taken in parallel. Sab, Sabouraud medium. (B) Capsule sizes at the different time points.

study with the wild-type strain (H99), the cyclin mutant, and the corresponding reconstituted strain.

Capsule enlargement *in vitro*. We first investigated whether capsule size was affected in the cyclin mutant. For this purpose, we measured the total cell size, the cell body size (delimited by the cell wall), and the capsule size after growth under regular conditions (Sabouraud liquid medium) or in capsule-inducing medium (10% Sabouraud medium [pH 7.3]). As shown in Fig. 4, the *cln1*

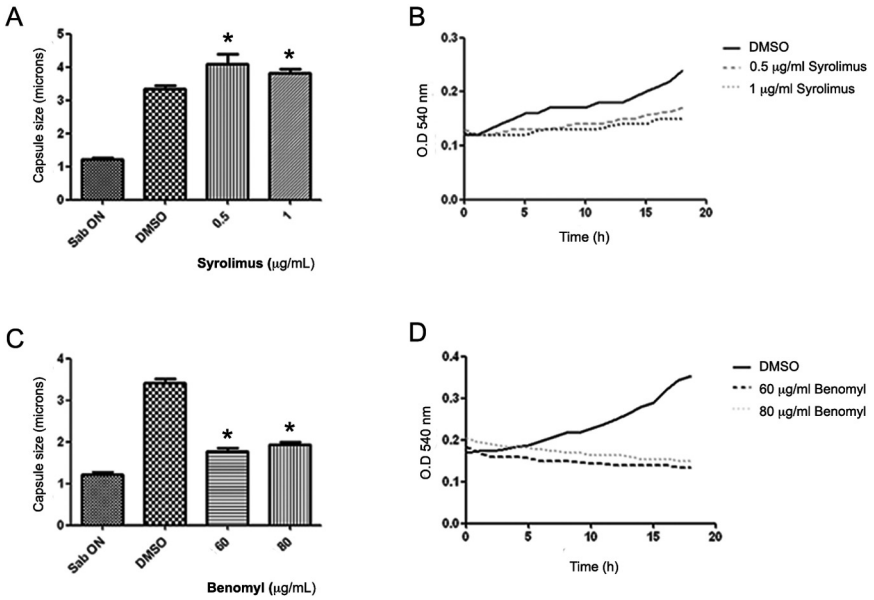

FIG 2 Capsule enlargement in the presence of cell cycle inhibitors. Bars show the means ± standard deviations (SD) of the capsule sizes measured from cultures incubated with different concentrations of sirolimus (rapamycin) (A) or benomyl (C). *, $P < 0.05$. (B and D) Growth curves of *C. neoformans* in capsule-inducing medium with the different concentrations of sirolimus (B) and benomyl (D). Cultures containing DMSO were used as controls.

mutant had larger cell body size than the wild-type and reconstituted strains. The mutant had also significantly larger capsule size than the other two strains, suggesting that, in fact, capsule size was coordinated with cell cycle progression.

Time-lapse microscopy revealed differences in G_1 length and budding time in the *cln1* mutant. G_1/S cyclin mutants showed a delay in the initiation of DNA replication (40), so we investigated if the mutant also had a delay in the appearance of the bud. For this purpose, we performed live imaging and measured the time of cell growth and budding. We focused on nascent daughter cells, not on mother cells, since the latter cells have already reached the size that induces cell cycle progression and the G_1 phase is almost absent after the separation of the bud (41, 42). The analysis of these videos showed that more than 50% of the cells in the mutant strain population had defects in cell cycle progression. Daughter cells showed aberrant shapes and remained attached to the mother cell, and thus, it was difficult to quantify the time required for these daughter cells to bud again. However, the other 50% of the daughter cells managed to completely separate from the mother cells and showed a significant delay in the appearance of the new bud compared to the wild-type strain (61 ± 3 min versus 98 ± 12 min; $P < 0.05$) (see Movies S2 and S3 in the supplemental material).

The *cln1* mutant showed increased vesicle production. Capsule synthesis has been related to the secretion of vesicles with capsular polysaccharide and other components inside (43, 44). Therefore, we investigated whether *cln1* had an enhanced ability to secrete vesicles during capsule growth. We isolated and estimated the amount of vesicles from the supernatant of the cultures by using a fluorometric assay (43, 44). Using this approach, we observed that *cln1* produced more extracellular vesicles than the wt and reconstituted strains (Fig. 5A). In parallel, we quantified the amount of sterol present in the vesicle preparation using high-performance thin-layer chromatography (HPTLC) as an independent parameter that reflects vesicle secretion. In agreement with the fluorometric assay, we found that *cln1* had higher sterol content than the wild-type and reconstituted strains (Fig. 5B and C).

Analysis of differentially accumulated proteins in *cln1* during capsule enlargement. To investigate the mechanisms by which the *cln1* mutant produces larger capsules relative to the wild-type strain, we compared the accumulation of proteins in these two strains during the capsule enlargement process. We performed protein extraction from wt and *cln1* cells incubated under capsule-inducing conditions for 6 h (see Materials and Methods). The analysis was performed with 3 independent replicates. Protein extracts were processed by difference gel electrophoresis (DIGE). A difference of ±1.5-fold change in protein accumulation was considered statistically significant ($P < 0.05$). All possible proteins and their relative abundance were represented in a heat map (Fig. 6). Thirty possible proteins were automatically matched. Twenty-six proteins out of 30 could be cut using ImageQuant v 5.1 software (GE Healthcare) after the gel had been stained with colloidal Coomassie blue (CCB). These 26 proteins were imported to the Oracle database, and 19 of them were identified by mass spectrophotometry with a 4800 matrix-assisted laser desorption ionization–tandem time of flight (MALDI-TOF/TOF) mass spectrometer. Finally, sequences were identified by comparison to *Cryptococcus neoformans* database available at the Broad Institute.

As shown in Table 1, some proteins involved in meiosis and budding were less abundant in the *cln1* mutant than in the wt strain (H99). However, proteins such as malate synthase (which is involved in the glyoxylate cycle and allows the yeast to get energy from fatty acids) and other proteins related to glucose and xylose metabolism (i.e., transketolase and aldoketolase) were more abundant in the *cln1* mutant than in the wt strain.

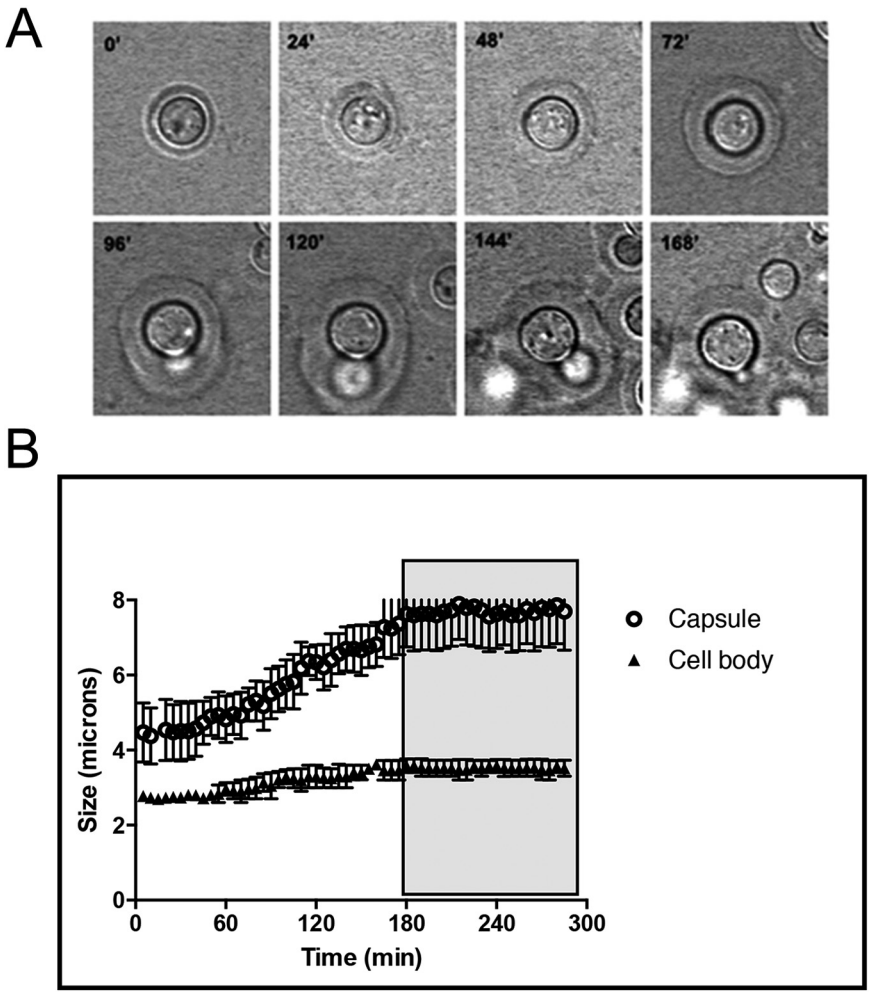

FIG 3 Capsule growth visualization by time-lapse microscopy. Capsule enlargement was observed based on the capsular "quellung" reaction produced by the 13F1 MAb. (A) Sequence of frames showing capsule and cell body enlargement. (B) The rate of capsule and cell body growth was determined by linear regression analysis of lengths as a function of time. The capsule enlargement speed was 8.8 nm/min, and the cell body enlargement speed was 3.6 nm/min. A plateau in capsule and cell body size is observed following yeast replication (boxed in gray).

Virulence and capsule variations of the *cln1* strain during *G. mellonella* infection. Since the *cln1* strain showed a temperature-sensitive growth defect, we tested its potential virulence in *Galleria mellonella* (Fig. 7A). We chose this model because virulence can be assessed at different temperatures (45). The cyclin mutant strain was completely avirulent at 37°C ($P < 0.05$). In contrast, at lower temperature, the mutant was as virulent as the wild-type strain ($P > 0.05$). Interestingly, *cln1* yeast cells recovered after 3 days of infection from larvae incubated at 30 and 37°C had a larger cell and capsular size than the wt strain (Fig. 7B). In all cases, the *cln1*::*CLN1* strain restored the virulence phenotype.

We also tested the degree of phagocytosis using the *G. mellonella* model. After 2 h of the administration of the yeasts to the larvae, hemocytes showed reduced phagocytosis of *cln1* strain compared to the wt and *cln1*::*CLN1* strains (1% ± 0.7% versus 19% ± 3% and 13% ± 1%; $P < 0.05$) (Fig. 7C).

Macrophage and *C. neoformans* interaction. Phagocytosis assays were also performed with the macrophage-like cell line RAW 264.7. Cells from the *cln1* mutant were less efficiently phagocytosed by murine macrophages than the wt strain (41% ± 6% versus 88% ± 2%, respectively). Furthermore, intracellular replication was determined using time-lapse microscopy. The *Cryptococcus neoformans* wt strain was able to replicate within 30 to 40% of infected macrophages. In contrast, in macrophages infected with the *cln1* mutant, we only observed fungal replication in <10% of the cases.

DISCUSSION

Our study provides evidence that capsule enlargement in *C. neoformans* is coordinated with the cell cycle. We hypothesized that *C. neoformans* enlarges its capsule during G_1 phase for the following reasons. Several studies have already shown that capsule enlargement is induced in *C. neoformans* in low-iron medium (13), in the presence of CO_2 (15), in serum (11), in diluted Sabouraud medium (12), or in the presence of mannitol (14). Under each of these conditions, yeast cells grow more slowly—probably because they spend more time in G_1 phase. Furthermore, it is possible that the addition of capsule during $S/G_2/M$ phases could interfere with the process of budding and daughter cell separation, thus providing another reason for linking capsule growth to G_1 phase of the

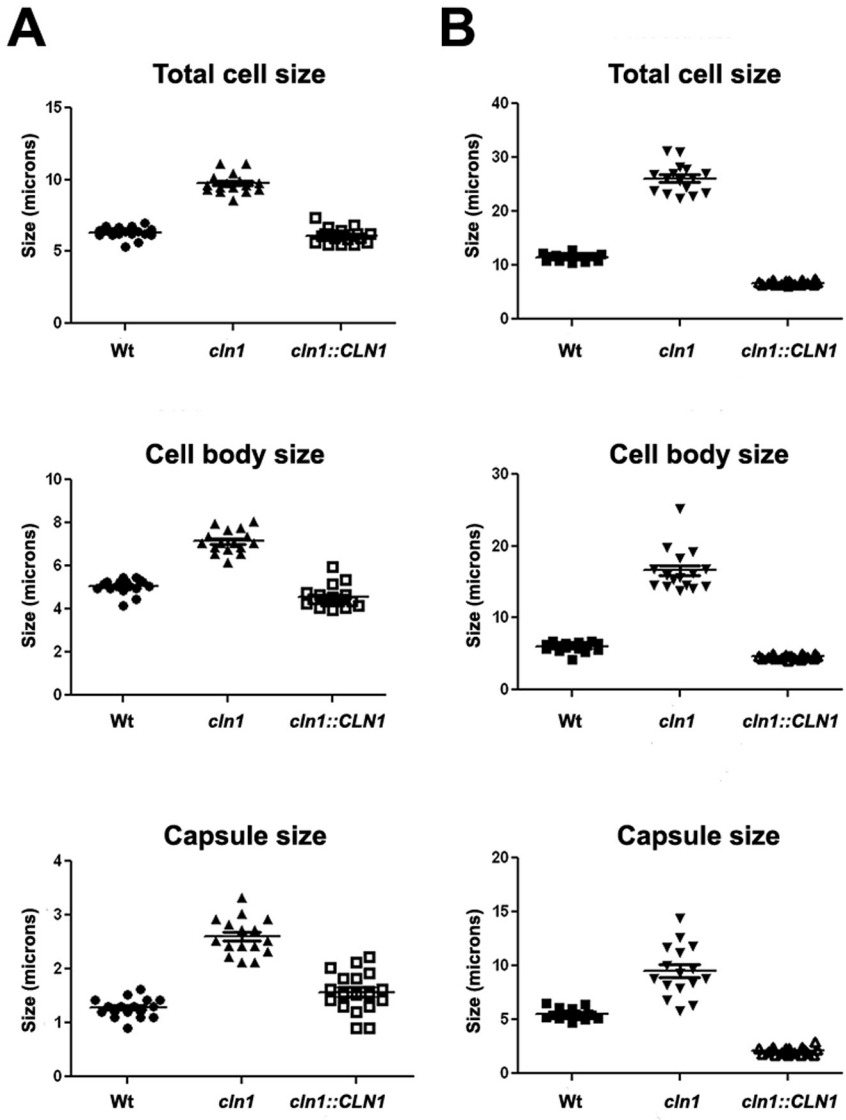

FIG 4 Morphogenesis of wt, *cln1*, and *cln1*::*CLN1* strains from *C. neoformans*. (A and B) Distribution of total cell size, cell body size, and capsule diameter of *C. neoformans* cells grown in Sabouraud medium (A) and in 10% Sabouraud medium buffered at pH 7.3 with 50 mM MOPS (B).

cell cycle. Moreover, it has been observed that during capsule growth, there is a correlation between the cell body size and capsule size (11, 23), suggesting that these two processes are in fact coordinated.

Using different techniques (flow cytometry and live imaging), we confirmed the relationship between capsule growth and G_1 arrest. Interestingly, we observed that after capsule enlargement and bud separation, mother cells progressed normally through the cell cycle (fast appearance of a new bud with a very short G_1 phase), with the absence of further capsule growth. This result suggests that the G_1/S checkpoint is controlled, not only by cell body size but also by capsule size after capsule enlargement stimulation. This regulation might be dependent on the TOR pathway, since sirolimus, which also causes G_1 arrest (46), enhanced capsule growth. In budding yeast, the TOR pathway detects nutrient conditions and promotes cell growth and proliferation, which is also connected to cell size (47). Inhibition of the TOR pathway by sirolimus leads to arrest cryptococcal cells in G_1 phase, and thus cryptococcal cells have more time to enlarge their capsules. These results were confirmed by using another cell cycle inhibitor, such as benomyl. This drug has been described to arrest cells in M phase due to the loss of microtubule function (48). Our results demonstrate a link between cell cycle and capsule growth, and open a new perspective to understand the regulation of this process.

We also investigated capsular phenotypes in a mutant that had a G_1/S cyclin disrupted (*CLN1*) and which was available at the ATCC. Parallel studies have phenotypically confirmed the role of this gene as coding for a G_1/S cyclin (31). In preliminary experiments, this mutant manifests an elongated G_1 phase and exhibited a larger capsule relative to the wt strain under capsule-inducing conditions, confirming that capsule growth was coordinated with the cell cycle. The *cln1* mutant produces more extracellular vesicles than wt and reconstituted strains, which confirmed the hypercapsular phenotype of *cln1*, since it is known that transport of vesicles in *C. neoformans* is linked to capsule production (44).

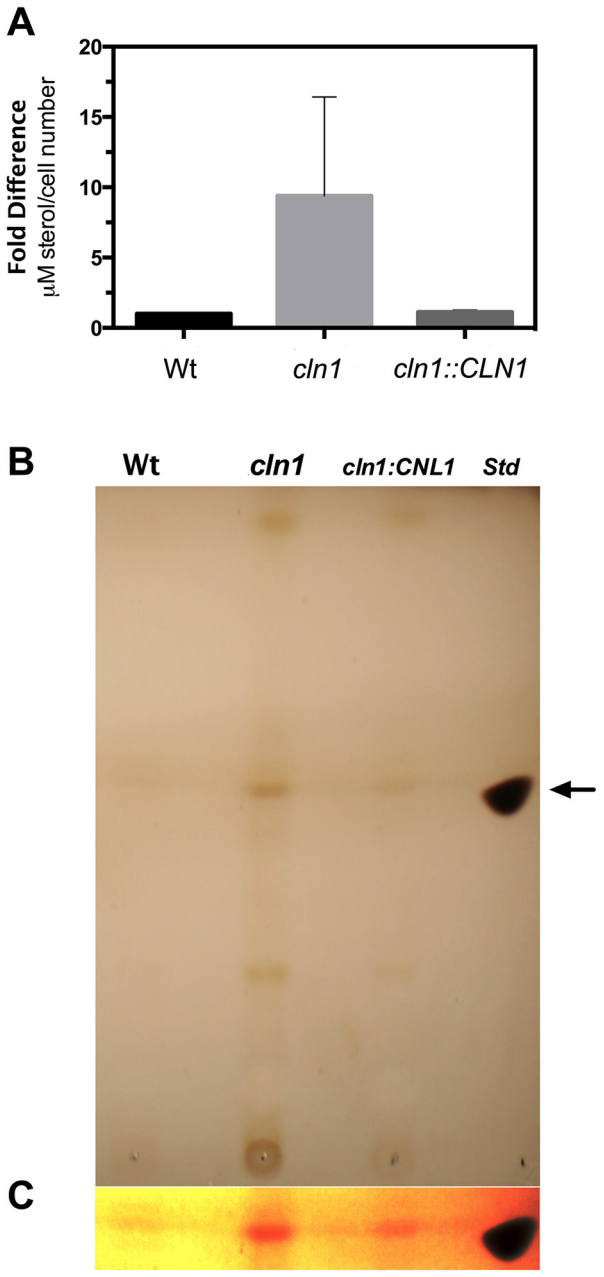

FIG 5 The *cln1* mutant shows increased production of extracellular vesicles. (A) Comparative analysis of vesicle production based on an indirect sterol-based vesicle quantification of fractions obtained from the wt, mutant, and reconstituted *C. neoformans* strains, using a fluorometric assay kit. Error bars represent standard deviations of 3 independent experiments. (B) Comparative analysis of the sterol content in vesicle preparations using HPTLC. An arrow indicates the migration of an ergosterol standard (Std). The result is representative of 2 independent analyses showing similar results. (C) Contrast image of the area highlighted with the arrow in panel B to emphasize the differences in band intensity among strains.

Besides, the *cln1* mutant also manifested a defect in the width of the neck between the mother and the bud, which was significantly narrower in the WT strain than in the cyclin mutant (31). This finding had been already reported and could also explain the delay in budding since it restricts the movement of plasma membrane proteins and cell wall material (31). However, our results should not be interpreted as if any condition that enlarged G_1 phase results in capsule growth, since an inducing signal is required (i.e., mannitol, serum, CO_2, or nutrient deprivation). In this regard, little is known about the stimuli that trigger capsule induction, and further studies are required to understand the changes that occur in the cell during capsule growth.

Our initial characterization of the mutant using time-lapse microscopy demonstrated that the mutant had an elongated G_1 phase, supporting its role in the regulation of the transition from G_1 to S phase. In budding yeasts, the G_1 phase in the mother cell is very short because it has already reached the proper size for cell division. However, the daughter cell of the *cln1* mutant exhibits a longer G_1 phase, until it reaches a cell size that triggers the initiation of the cell cycle (Start) (41, 42, 49). Furthermore, we observed a significant delay in budding in the *cln1* mutant strain compared to wt or reconstituted strains, which is in agreement with previous findings (50, 51). This phenomenon could imply that *cln1* mutation may cause a delay in a later part of the cell cycle, so that buds grew large before they separate (52, 53). Alternatively, it could mean that enlarged mother cells require more time to duplicate all of their cytoplasmic content during budding because of the larger size of the cells.

Cell cycle and G_1 cyclins are also involved in the morphogenesis and differentiation of different yeast species, such as *Candida albicans*, *Saccharomyces cerevisiae*, and *Ustilago maydis* (39, 54, 55). Our results are in agreement with these findings, since capsule enlargement can be considered in *C. neoformans* as a morphological transition that involves multiple cellular changes, in particular, induction of changes in gene expression that result in a dramatic accumulation of new polysaccharide in the capsule (20, 21, 56–58). Cyclins are a highly conserved family of proteins that are involved in multiple processes in the cell through regulation of specific protein kinases. During cell cycle progression, cyclins bind and regulate the activity of the cyclin-dependent protein kinases (CDKs). There are several cyclins that control different parts of the cell cycle through activation of appropriate CDK partners (59). However, it has been reported that these cyclins could be involved in different signaling pathways, including fungal development, toxin metabolism, and pathogenicity (39, 60). Absence of Cln1 results in a longer G_1 phase, suggesting that this protein is involved in the regulation of this transition. However, full identification of the biochemical function of this protein will require further studies to elucidate whether this protein binds to Cdk1 or to another protein kinase.

Proteomic analysis showed that some proteins related to meiosis and budding were in smaller amounts in the *cln1* mutant than in the wt strain. In the *cln1* mutant, proteins related to the glyoxylate cycle and glucose metabolism were more abundant than in the wt strain, which suggests that *cln1* cells are more metabolically active. This result is in agreement with the idea that G_1 is the phase the most metabolically active of the cell cycle. Therefore, our results suggest a model in which factors that elongate G_1 allow cells to stay in G_1 for a longer time and thus increase their capsules.

The protein Wos2 was also more abundant in the *cln1* mutant than in the wt strain. This protein was described as a homolog of P23 in *Schizosaccharomyces pombe* that is involved in cell cycle progression, so its expression decreases when cells enter stationary phase or are grown under nutrient limitation conditions (61). Besides, different heat shock proteins appeared differently accu-

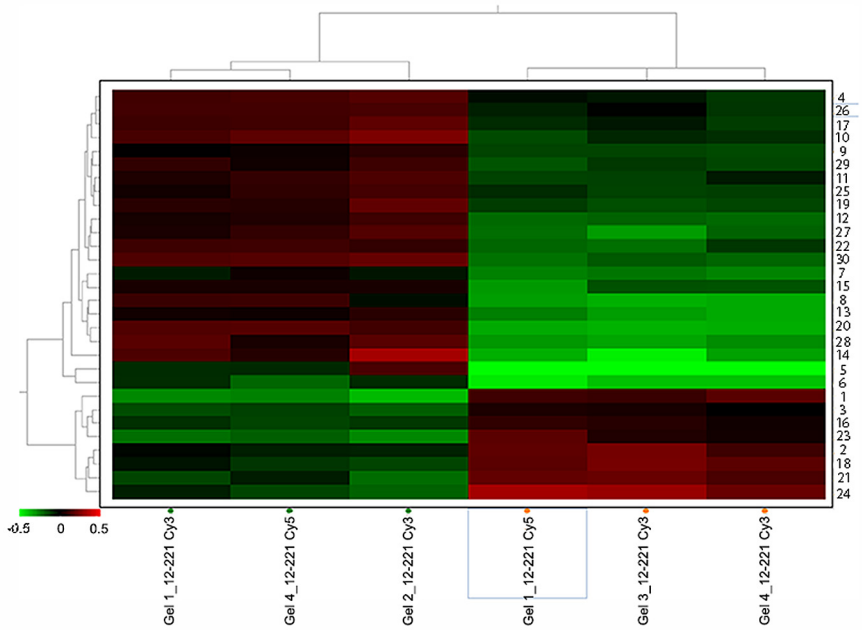

FIG 6 Relative abundance of proteins accumulated in the *cln1* mutant under capsule-inducing conditions. The upper dendrogram shows the relationship among individual gels, while the left dendrogram shows the relationship among proteins. Hierarchical clustering analysis (HCA) was performed to obtain the values of abundance of every spot, which were then represented in a heat map. Different red spots show a positive relative abundance (*cln1* mutant/H99 ratio), while different green spots show a negative relative abundance.

mulated. Some of them were more abundant in the *cln1* mutant than in the wt strain, such as the heat shock protein Hsp90, which is involved in the response to heat shock and is required for the viability of the cells (62). In contrast, other heat shock proteins appeared less abundant in the *cln1* mutant than in the wt strain, such as Hsp70, which has been linked to the expression of laccase in *C. neoformans* (63).

The cyclin mutant exhibited virulence defects, especially at 37°C, which are related to its reduced growth at this temperature. Interestingly, yeast cells recovered from infected larvae showed an enlarged capsule compared to those observed *in vitro* (45, 64). This result correlates with the fact that cryptococcal cells can remain in the host in a latent state without being eliminated (reviewed in reference 65). *Cryptococcus neoformans* is an intracellular fungal pathogen, which means it can persist in hosts inside macrophages (66–70). However, we have observed that the *cln1* mutant is poorly phagocytosed by *Galleria* hemocytes, possibly because its larger size impairs its internalization by phagocytic cells, which correlates with a defect in virulence. Furthermore, this hypothesis was confirmed by the results observed from the *in vitro*

TABLE 1 List of proteins identified by mass spectrophotometry[a]

Spot	Protein identification	*cln1* mutant/H99 ratio (fold change)	ORF
1040	Transketolase	3.74	CNAG_07445
617	Heat shock proteín 90	3.59	CNAG_06150
2002	Wos2 (p21)	2.76	CNAG_07558
861	Malate synthase	2.54	
2228	Phosphopyruvate hydrogenase	2.37	CNAG_03072
1427	Aldoketoreductase	1.94	CNAG_01257
974	Chaperone	1.92	CNAG_01750
1222	Ornithine carbamyltransferase	1.8	CNAG_02813
1062	Aminotransferase	1.79	CNAG_02853
860	Malate synthase	1.7	CNAG_05653
1149	Adenylsuccinate synthase	1.68	CNAG_02858
2227	Phosphogluconate dehydrogenase	1.67	CNAG_07561
598	Heat shock protein	1.59	CNAG_05199
915	UTP-glucose-1-phosphate uridyltransferase	1.51	CNAG_02748
1133	Methione adenosyltransferase	−1.52	CNAG_00418
584	Heat shock protein 70	−1.55	CNAG_01727
532	Heat shock protein	−1.69	CNAG_06443
1473	Budding-related protein	−2.08	CNAG_04194
531	Meiosis-related protein	−2.71	CNAG_00995

[a] The first and second columns indicate the proteins. The third column shows the fold change in accumulation of the protein between wt and *cln1* strains. The last column is the corresponding ORF for each protein when a BLAST protein-protein comparison was performed in the *C. neoformans* database of the Broad Institute

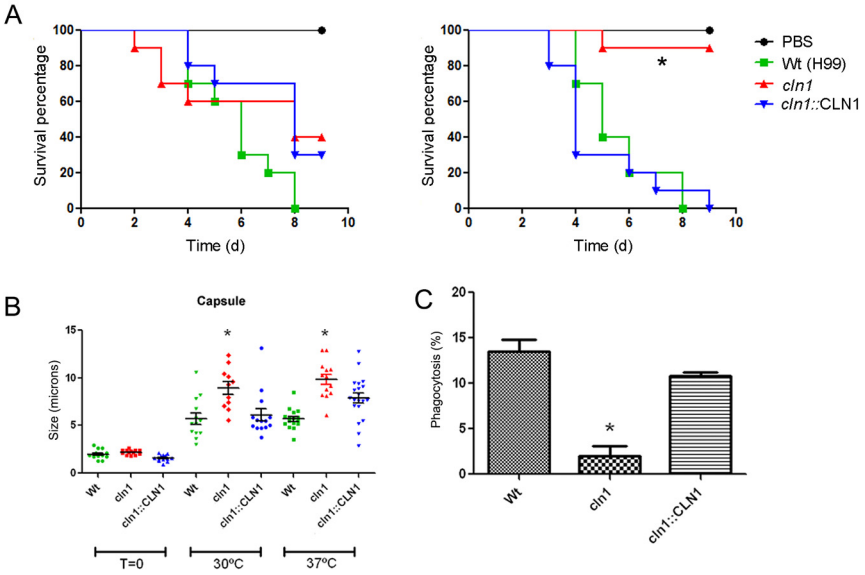

FIG 7 *In vivo* model of the effect of *cln1*. (A) Survival curves of *G. mellonella* infected with 10^6 cells of *C. neoformans* strains at 30°C (left) and 37° C (right) (B) Capsule sizes of yeast cells recovered from *G. mellonella* after 3 days of infection at 30 and 37°C. (C) Phagocytosis was performed at a 2:1 ratio of yeast cells to macrophages (see Materials and Methods). Bars show the mean ± SD phagocytosis of *C. neoformans* cells after 2 h at 37°C. *, $P < 0.05$.

interaction between murine macrophages and wt and *cln1* mutant strains of *C. neoformans*. Besides, the reduced capability of the *cln1* mutant to replicate within macrophages could explain its decrease in virulence. During the interaction between the *cln1* mutant and murine macrophages, extrusion was only observed in one case, which leads us to think that, finally, macrophages are able to control the infection and eliminate the phagocytosed yeast cells.

In summary, our results demonstrate a link between cell cycle and the regulation of the size of the main virulence factor of *C. neoformans*. We propose a model for capsule growth in which capsule induction stimulus is followed by a transient arrest in G_1 that induces capsular enlargement until a certain size is reached, which then triggers the progression of the cell cycle. We have also demonstrated that the absence of Cln1 results in reduced virulence, so cryptococcal factors that regulate the cell cycle could offer a good target to develop new antifungal compounds.

MATERIALS AND METHODS

Strains and culture conditions. *Cryptococcus neoformans* var. *grubii* strain H99 (71) and the *cln1* mutant strain CNAG_06092, obtained from a collection of mutants deposited at the ATCC by H. D. Madhani (20), were used in this study. The strains were routinely grown in liquid Sabouraud medium (Oxoid, Ltd., Basingstoke, Hampshire, England) at 30°C or 37°C with moderate shaking (150 rpm). To induce capsule growth, the cells were transferred to 10% Sabouraud medium buffered at pH 7.3 with 50 mM MOPS (morpholinepropanesulfonic acid) buffer (Sigma-Aldrich, St. Louis, MO) at 30°C or 37°C with shaking (12). Murine macrophage-like cells (72) were grown in feeding medium, which contains Dulbecco's modified Eagle's medium (Lonza, Verbiers, Belgium) supplemented with 10% heat-inactivated fetal bovine serum (FBS) (HyClone-Perbio), 10% NCTC medium (Sigma-Aldrich, Steinheim, Germany) and 1% nonessential amino acids (Sigma-Aldrich, Steinheim, Germany). Macrophages were regularly maintained at 37°C in a 5% CO_2-enriched atmosphere.

Nuclear staining and FACS analysis. Measurement of DNA content by flow cytometry was performed as described in reference 52 with minor modifications. Aliquots were taken at different time intervals from 10% Sabouraud medium in MOPS buffer and pelleted by centrifugation. Cells were suspended in 70% ethanol and kept overnight at 4°C for fixation. The cells were washed twice with distilled water and finally suspended in 2 ml of a mixture of 20 mM sodium citrate, 50 mM EDTA, and 0.45 mM sorbitol (pH 5.5). After 1 h of incubation at 30°C, RNase (Sigma-Aldrich, St. Louis, MO) was added at a final concentration of 10 μg/ml, and the tubes were kept at 30°C for 2 h.

Propidium iodide was added to a final concentration of 5 μg/ml, and samples were taken to the cytometer. Samples without propidium iodide were used in parallel as negative controls. Stained cells were observed under the fluorescence microscope, and DNA content was measured using a FacsCalibur flow cytometer (BD Biosciences, Woburn, MA). Flow cytometry data were processed using CellQuest (BD Biosciences) and FlowJo (Tree Star, Inc., Ashland, OR) software.

Capsule growth in the presence of cell cycle inhibitors. *Cryptococcus neoformans* strain H99 cells were grown in 5 ml of Sabouraud medium at 30°C with moderate agitation. Cells were washed and transferred to 10% Sabouraud medium in MOPS buffered at pH 7.3 containing sirolimus (Sigma-Aldrich, St. Louis, MO) at different concentrations (0, 0.5, and 1 μg/ml), which induces G_1 arrest. In addition, benomyl (Sigma-Aldrich, St. Louis, MO), which causes M arrest, was also tested for its effect on capsule growth. Cells were grown in Sabouraud liquid medium at 30°C overnight and then washed and incubated in 10% Sabouraud medium in MOPS (pH 7.3) containing different benomyl concentrations (0, 60, and 80 μg/ml). Cultures were incubated at 30°C overnight, and suspensions of India ink were photographed and measured as explained above. DMSO was added to the control cultures (without drugs). In addition, propidium iodide (5 μg/ml) was added to the cells after incubation with the drugs to verify that any possible effect on capsule growth was not due to lack of viability. Heat-killed cells (65°C, 1 h) were used as a positive control.

To confirm that the drugs had an effect on the cells, we performed growth curves in 10% Sabouraud liquid medium buffered in MOPS at pH 7.3 containing the different concentrations of the drugs mentioned above in a 96-well plate (Costar, NY) during 18 h at 30°C using an iEMS spectrophotometer (Thermofisher). The optical density at 540 nm (OD_{540}) was measured every hour, and graphs were plotted using Graph Pad Prism 5.

***In vivo* capsular growth visualization using time-lapse microscopy.** Cells from the H99 strain were grown overnight in 10 ml of Sabouraud

medium at 30°C under constant agitation. The cells were then washed 3 times with phosphate-buffered saline (PBS), and the density was enumerated using a hemocytometer. Approximately 10^4 cells were placed in a Lab-Tek chambered coverglass (Thermo, Fisher Scientific, Rochester, NY) containing 100 μl of capsule-inducing medium (10% Sabouraud medium buffered in 50 mM MOPS) and supplemented with 20 μg/ml of IgM MAb 13F1 (73). The chamber slide was placed in a temperature-controlled microscope chamber adjusted to 37°C. Image acquisition was done at 5-min intervals with a 40× differential inference contrast (DIC) objective in an SP5 confocal inverted microscope equipped with a camera. Images were processed using Leica Microsystems and ImageJ software. Capsule and cell body dimensions were determined from time-lapse microscopy images using Adobe Photoshop. Capsule radial length was calculated by subtracting the length of the cell body from the diameter of the whole cell, capsule included. Determination of the capsule and cell body growth rate was done by linear regression of a length versus time plot.

Identification of G_1/S cyclins by homology with the corresponding cyclin from *Ustilago maydis*. The Cln1 protein sequence from *Ustilago maydis* (39) was used to perform a BLAST comparison against the *C. neoformans* H99 strain genome deposited at the Broad Institute (http://www.broadinstitute.org/annotation/genome/cryptococcus_neoformans/MultiHome.html). In this way, we identified ORF CNAG_06092, which was already annotated as coding for a putative cyclin. Moreover, this gene has been characterized as encoding a G_1/S cyclin protein (31) and consequently was denominated *CLN1*.

Reconstitution of the *CnCLN1* gene. The reconstituted strain (*cln1*::*CLN1*) was created by biolistic DNA delivery. Genomic DNA from wild-type *C. neoformans* var. *grubii* containing the full-length *CnCLN1* gene was amplified by PCR using Phusion high-fidelity DNA polymerase (Finnzymes, Espoo, Finland) using the primers NEOCLN1 (5′ GTCATA GCTGTTTCCTGGAGCAGGTCTCCTCAACGTCTT 3′) and CLN13′3 (5′ AAGTATCACCGTCCAGTTCGTG 3′). The neomycin resistance marker (74) was amplified from the pPzp plasmid (75) using the primers CLN1MKRf (5′ CTTAGCCGTCTCATAACGCGACCCAGTCACGACG TTGTA 3′) and NEOCLN1r (5′ AAGACGTTGAGGAGACCTGCTCCA GGAAACAGCTATGAC 3′). The *C. neoformans* gene cassette was created by fusion PCR (76, 77) using the CLN1MKRf and CLN13′3 primers. Biolistic transformation was performed as in reference 76 using a Bio-Rad PDS 1000/He Biolistic PDS machine. Colonies were selected on YPD plates containing 100 μg/ml of Geneticin, and integration of the gene was confirmed by PCR.

Estimation of G_1-phase length by real-time microscopy. Suspensions of *C. neoformans* strains were prepared in Sabouraud liquid medium at 10^4/ml from overnight cultures. Wells from a 96-well plate were coated with 50 μl of a stock solution of MAb 18B7 at a final concentration of 0.2 μg/ml and incubated for 1 h at room temperature. Then mAb18B7 was removed, 100 μl from the yeast suspension was added, and the mixture was incubated at 30°C under a Leica DMI 4000B microscope. Photographs were taken every 2 or 3 min using the 20× objective. The videos generated by the Leica software were exported as AVI documents and processed with ImageJ software (NIH; http://rsb.info.nih.gov/ij). The G_1 phase was calculated by counting the frames from the appearance of the first daughter cell until the same daughter cell began to bud again.

Analysis of extracellular vesicle production. The wild type, *cln1* mutant, and reconstituted strains were grown in 1-liter cultures of capsule-inducing medium under constant agitation for 2 days at 30°C. Culture supernatants, containing extracellular vesicles, were cleared by centrifugation at 5,000 × *g* (25 min, 4°C). Supernatants were then collected and passed through a 0.8-μm-pore filter membrane. The filtered volume was centrifuged at 100,000 × *g* for 1 h at 4°C using a 45 Ti rotor. Vesicle pellets were washed 3 times with sterile-filtered cold PBS, with the sample centrifuged each time at 100,000 × *g* for 1 h at 4°C.

Vesicle production was assayed by measuring the concentration of sterols (structural components and markers of fungal extracellular vesicles and vesicle membranes [44]) by a quantitative fluorometric kit (Amplex red sterol assay kit; Molecular Probes) and by high-performance thin-layer chromatography (HPTLC).

For sterol quantification using the Amplex kit, the resulting pellets were suspended in 500 μl of PBS and processed according to the manufacturer's instructions. The sterol concentration was normalized by culture's cell density.

For HPTLC, the vesicle pellets were extracted with 3 sample volumes of methanol-chloroform (1:1). The mixtures were homogenized by sonication. The lower phase (chloroform) was recovered, dried, and suspended in methanol for analysis by HPTLC. The volume of methanol used to resuspend the lipid material was proportional to the cell density of the cultures. Thirty microliters of the samples was loaded into HPTLC silica plates (Si 60F254s; LiChrospher, Merck, Germany) and separated using the mobile-phase hexane-ether-acetic acid (80:40:2 [vol/vol/vol]). Sterol spots were identified by spraying the plate with a ferric chloride solution and heating at 100°C for 3 to 5 min.

Proteomics. To investigate the different patterns of protein accumulation between the *cln1* mutant and wt strain, we performed proteomics. Yeast cells were grown in 10 ml of Sabouraud liquid medium overnight at 30°C. Then the cells were transferred to capsule-inducing medium (10% Sabouraud in 50 mM MOPS [pH 7.3]) at a final cell density of 10^7 cells/ml. After 6 h of incubation at 30°C, cultures were centrifuged at 3,500 × *g* for 10 min, and the pelleted cells were suspended in protein lysis buffer (5 mM EDTA, 1× Complete protease inhibitor cocktail [Roche, Indianapolis, IN] in TE buffer [10 mM Tris-HCl at pH 8.1, mM EDTA]). Next, two aliquots of 1 ml were separated in 2-ml tubes, and 425- to 600-μm Ø glass beads (Sigma-Aldrich, St. Louis, MO) were added. Cell rupture was carried in a Fast-Prep for 6 cycles of 20 s with 4-min intervals in ice. Finally, tubes were centrifuged for 10 min at 4°C, and supernatants were collected and kept at 4°C until protein determination using the Bradford protein assay (Bio-Rad, Munich, Germany) was performed.

Protein samples were analyzed at the Proteomics Facility at the UCM-UPM (a member of the ProteoRed-ISCIII network). Samples were purified with the 2D-Clean Up cleaning kit (GE Healthcare). Bradford quantification was confirmed by 10% SDS-PAGE, and samples were stained with colloidal Coomassie blue (CCB).

Next, the 4 replicates of 100 μg from each sample (*cln1* mutant and H99) were mixed and loaded in a two-dimensional (2D)-PAGE gel. To visualize the proteins, gels were stained with CCB and scanned. Half of the biological replicates were stained with Cy3 and the other half with Cy5. Then the gels were scanned in a Typhoon Trio fluorescent scanner (GE Healthcare) using filters corresponding to each fluorochrome (excitation/emission: Cy3, 532/580; Cy5, 633/670; Cy2, 488/520 nm). Once scanned, gels were stained with CCB.

Images were cut with ImageQuant v 5.1 software (GE Healthcare) and imported to the Oracle database. After the automatic matching of the putative proteins, manual corrections and matching were carried out. Different statistical analyses were performed, such as principal-component analysis and cluster analysis, to obtain the final number of proteins to be identified by mass spectrophotometry in a 4800 MALDI-TOF/TOF mass spectrometer. The identification of picks was performed using the NCBI database with taxonomic restriction in yeast.

***Galleria mellonella* survival experiments.** *Galleria mellonella* larvae (Alcotan, Valencia, Spain) were infected as described in references 45 and 64. Briefly, larvae were selected to weigh between 0.3 and 0.5 g and to be free of any dark marks. Then the pro-leg area was cleaned with 70% ethanol using a swab. The larvae were inoculated with 10 μl of a yeast suspension prepared at 10^8/ml in PBS containing 50 μg/ml of ampicillin by an injection using a 26-gauge needle with Hamilton syringes. The syringes were prepared by cleaning them with diluted bleach and ethanol. After injection, caterpillars were incubated in 90-mm plastic petri dishes (Soria Genlab, SA, Madrid, Spain) at 37 or 30°C, and the number of dead caterpillars was scored every day. A group of 20 larvae were inoculated with PBS with 50 μg/ml of ampicillin in each experiment to monitor

killing due to physical injury, and another group of 20 caterpillars without any manipulation were used in parallel as untreated controls.

Isolation of *C. neoformans* cells from *G. mellonella*. To isolate the yeasts from *G. mellonella*, larvae were smashed using cell strainers with a 100-μm pore size (BD Falcon, Erembodegem, Belgium) and 5-ml syringe plungers (BD Plastipak, Madrid, Spain) (64). Homogenates were collected in 1 ml of PBS, and samples were washed twice and suspended in 150 μl of PBS.

Fungal cells were suspended in India ink (Remel Bactidrop, Lenexa, KS), observed by microscopy, and photographed using a Leica DMI 3000B microscope. In parallel, pictures of the cryptococcal cells grown overnight in Sabouraud liquid medium were taken to control for cell size prior to infection ($T = 0$). Cell and capsule sizes were measured using Adobe Photoshop 7.0 (San Jose, CA). Total cell size was defined as the diameter of the complete cell, including the capsule. Capsule size was calculated as the difference between the diameter of the total cell and the cell body diameter, defined by the cell wall.

***In vivo* phagocytosis assays.** Yeast cells were grown in liquid Sabouraud medium as described above and stained with Calcofluor white (Sigma-Aldrich, St. Louis, MO) at 10 μg/ml for 30 min at 37°C. After incubation, cells were washed twice with PBS and suspended at 10^8 cells/ml. Larvae were infected with 10 μl of the inoculum (10^6 cells) and incubated at 37°C. After 2 h, hemolymph was collected in microcentrifuge tubes containing 100 μl of PBS and centrifuged at 1,500 $\times$ *g* for 3 min. Pelleted hemocytes were suspended in 200 μl of PBS and placed on coverslips for 20 min to allow the cells to adhere. Coverslips were placed on the slides with Fluoromount G (Southern Biotech), and the number of hemocytes with internalized *C. neoformans* cells was enumerated using a Leica DMI 3000B fluorescence microscope. Phagocytosis was expressed as the percentage of hemocytes that contained yeast cells. Experiments were performed on different days in triplicates.

Phagocytosis with murine macrophages and Giemsa staining. Phagocytosis using the murine macrophage cell line RAW 264.7 and Giemsa staining was done as described in reference 78. Using a Leica DMI 3000B microscope, 5 pictures per well were taken to count the total number of macrophages and the number of macrophages with intracellular yeasts. The phagocytosis percentage was calculated as the number of infected macrophages divided by the number of total macrophages multiplied per 100.

Live imaging of the interaction between murine macrophages and *C. neoformans*. After phagocytosis experiments using RAW 264.7 macrophages, performed as described above, the nonphagocytosed yeasts were removed by extensive washing with macrophage feeding medium. The 96-well plate (MatTek, Ashland) was placed under a Leica SP5 confocal microscope, and pictures were taken using a 20$\times$ objective in a 5% CO_2 environment at 37°C. This motorized microscope allows the taking pictures of different wells in the same experiment. In that sense, two videos for the wt strain (H99) and 2 videos for the *cln1* mutant were obtained in parallel. Pictures were taken every 3 min for around 12 h. The videos generated by the Leica software were exported as AVI documents and processed with ImageJ software (NIH) (http://rsb.info.nih.gov/ij). The final videos were generated by merging 8 frames per s, with each frame taken every 3 min, which means that 1 s from the video is equivalent to 24 min of the experiment.

Statistical analysis. Survival data from *G. mellonella* experiments were analyzed by the Kaplan-Meier method using Graph Pad Prism 5 (La Jolla, CA). Every experiment was repeated three times, and the results were similar among all experiments. Scatter plot analysis of cell sizes was done with Graph Pad Prism 5 (La Jolla, CA), and statistical differences were assessed with a *t* test. A *P* value of <0.05 was considered significant. The *t* test was also performed to evaluate mean differences among the wt, *cln1*, and *cln1*::*CLN1* strains regarding the duration of the G_1 phase and the percentage of phagocytosis.

SUPPLEMENTAL MATERIAL

Supplemental material for this article may be found at http://mbio.asm.org/lookup/suppl/doi:10.1128/mBio.00945-14/-/DCSupplemental.

Movie S1, AVI file, 0.7 MB.
Movie S2, AVI file, 2.5 MB.
Movie S3, AVI file, 4.3 MB.

ACKNOWLEDGMENTS

O.Z. is funded by grants SAF2008-03761 and SAF2011-25140 from the Spanish Ministry for Economics and Competitivity. R.G.-R. is supported by an FPI fellowship (reference BES-2009-015913) from the Spanish Ministry of Science and Innovation. N.T.-C. is supported by an FPI fellowship (reference BES-2012-051837) from the Spanish Ministry for Economics and Competitivity. A.C. is supported by NIH grants HL059842-3, A1033774, A1052733, and AI033142. R.J.B.C. is supported by T32 AI07506 (NIH/NIAID).

REFERENCES

1. **Heitman J, Kozel T, Kwon-Chung K, Perferct J, Casadevall A.** 2011. *Cryptococcus*. From human pathogen to model yeast. ASM Press, Washington, DC.
2. **Mitchell TG, Perfect JR.** 1995. Cryptococcosis in the era of AIDS—100 years after the discovery of *Cryptococcus neoformans*. Clin. Microbiol. Rev. **8:**515–548.
3. **Park BJ, Wannemuehler KA, Marston BJ, Govender N, Pappas PG, Chiller TM.** 2009. Estimation of the current global burden of cryptococcal meningitis among persons living with HIV/AIDS. AIDS **23:**525–530. http://dx.doi.org/10.1097/QAD.0b013e328322ffac.
4. **Zaragoza O, Rodrigues ML, De Jesus M, Frases S, Dadachova E, Casadevall A.** 2009. The capsule of the fungal pathogen *Cryptococcus neoformans*. Adv. Appl. Microbiol. **68:**133–216. http://dx.doi.org/10.1016/S0065-2164(09)01204-0.
5. **Williamson PR.** 1997. Laccase and melanin in the pathogenesis of *Cryptococcus neoformans*. Front. Biosci. **2:**e99–e107.
6. **Casadevall A, Rosas AL, Nosanchuk JD.** 2000. Melanin and virulence in *Cryptococcus neoformans*. Curr. Opin. Microbiol. **3:**354–358. http://dx.doi.org/10.1016/S1369-5274(00)00103-X.
7. **Casadevall A, Perfect J.** 1998. Cryptococcus neoformans. ASM Press, Washington, DC.
8. **Zaragoza O, García-Rodas R, Nosanchuk JD, Cuenca-Estrella M, Rodríguez-Tudela JL, Casadevall A.** 2010. Fungal cell gigantism during mammalian infection. PLoS Pathog. **6:**e1000945.
9. **Okagaki LH, Strain AK, Nielsen JN, Charlier C, Baltes NJ, Chrétien F, Heitman J, Dromer F, Nielsen K.** 2010. Cryptococcal cell morphology affects host cell interactions and pathogenicity. PLoS Pathog. **6:**e1000953. http://dx.doi.org/10.1371/journal.ppat.1000953.
10. **Feldmesser M, Kress Y, Casadevall A.** 2001. Dynamic changes in the morphology of *Cryptococcus neoformans* during murine pulmonary infection. Microbiology **147:**2355–2365. http://mic.sgmjournals.org/content/147/8/2355.abstract.
11. **Zaragoza O, Fries BC, Casadevall A.** 2003. Induction of capsule growth in *Cryptococcus neoformans* by mammalian serum and CO_2. Infect. Immun. **71:**6155–6164. http://dx.doi.org/10.1128/IAI.71.11.6155-6164.2003.
12. **Zaragoza O, Casadevall A.** 2004. Experimental modulation of capsule size in *Cryptococcus neoformans*. Biol. Proced. Online **6:**10–15. http://dx.doi.org/10.1251/bpo68.
13. **Vartivarian SE, Anaissie EJ, Cowart RE, Sprigg HA, Tingler MJ, Jacobson ES.** 1993. Regulation of cryptococcal capsular polysaccharide by iron. J. Infect. Dis. **167:**186–190. http://dx.doi.org/10.1093/infdis/167.1.186.
14. **Guimarães AJ, Frases S, Cordero RJ, Nimrichter L, Casadevall A, Nosanchuk JD.** 2010. *Cryptococcus neoformans* responds to mannitol by increasing capsule size in vitro and in vivo. Cell. Microbiol. **12:**740–753. http://dx.doi.org/10.1111/j.1462-5822.2010.01430.x.
15. **Granger DL, Perfect JR, Durack DT.** 1985. Virulence of *Cryptococcus neoformans*. Regulation of capsule synthesis by carbon dioxide. J. Clin. Invest. **76:**508–516. http://dx.doi.org/10.1172/JCI112000.
16. **Anna EJ.** 1979. Rapid in vitro capsule production by cryptococci. Am. J. Med. Technol. **45:**585–588.
17. **Zaragoza O, Chrisman CJ, Castelli MV, Frases S, Cuenca-Estrella M,**

Rodríguez-Tudela JL, Casadevall A. 2008. Capsule enlargement in *Cryptococcus neoformans* confers resistance to oxidative stress suggesting a mechanism for intracellular survival. Cell. Microbiol. **10:**2043–2057. http://dx.doi.org/10.1111/j.1462-5822.2008.01186.x.

18. **Robertson EJ, Najjuka G, Rolfes MA, Akampurira A, Jain N, Anantharanjit J, von Hohenberg M, Tassieri M, Carlsson A, Meya DB, Harrison TS, Fries BC, Boulware DR, Bicanic T.** 2014. *Cryptococcus neoformans* ex vivo capsule size is associated with intracranial pressure and host immune response in HIV-associated cryptococcal meningitis. J. Infect. Dis. **209:** 74–82. http://dx.doi.org/10.1093/infdis/jit435.
19. **O'Meara TR, Norton D, Price MS, Hay C, Clements MF, Nichols CB, Alspaugh JA.** 2010. Interaction of *Cryptococcus neoformans* Rim101 and protein kinase A regulates capsule. PLoS Pathog. **6:**e1000776. http://dx.doi.org/10.1371/journal.ppat.1000776.
20. **Liu OW, Chun CD, Chow ED, Chen C, Madhani HD, Noble SM.** 2008. Systematic genetic analysis of virulence in the human fungal pathogen *Cryptococcus neoformans*. Cell **135:**174–188. http://dx.doi.org/10.1016/j.cell.2008.07.046.
21. **Haynes BC, Skowyra ML, Spencer SJ, Gish SR, Williams M, Held EP, Brent MR, Doering TL.** 2011. Toward an integrated model of capsule regulation in *Cryptococcus neoformans*. PLoS Pathog. **7:**e1002411. http://dx.doi.org/10.1371/journal.ppat.1002411.
22. **Bahn YS, Kojima K, Cox GM, Heitman J.** 2005. Specialization of the HOG pathway and its impact on differentiation and virulence of *Cryptococcus neoformans*. Mol. Biol. Cell **16:**2285–2300. http://dx.doi.org/10.1091/mbc.E04-11-0987.
23. **Zaragoza O, Telzak A, Bryan RA, Dadachova E, Casadevall A.** 2006. The polysaccharide capsule of the pathogenic fungus *Cryptococcus neoformans* enlarges by distal growth and is rearranged during budding. Mol. Microbiol. **59:**67–83. http://dx.doi.org/10.1111/j.1365-2958.2005.04928.x.
24. **Nandakumar H, Shankaramba KB.** 1990. Massive sequestration of the upper jaw: a case report. Br. J. Oral Maxillofac. Surg. **28:**55–56. http://dx.doi.org/10.1016/0266-4356(90)90014-C.
25. **Dirick L, Böhm T, Nasmyth K.** 1995. Roles and regulation of Cln-Cdc28 kinases at the start of the cell cycle of *Saccharomyces cerevisiae*. EMBO J. **14:**4803–4813.
26. **Forsburg SL, Nurse P.** 1991. Identification of a G_1-type cyclin puc1+ in the fission yeast Schizosaccharomyces pombe. Nature **351:**245–248. http://dx.doi.org/10.1038/351245a0.
27. **García-Muse T, Steinberg G, Perez-Martín J.** 2004. Characterization of B-type cyclins in the smut fungus *Ustilago maydis*: roles in morphogenesis and pathogenicity. J. Cell Sci. **117:**487–506. http://dx.doi.org/10.1242/jcs.00877.
28. **Stern B, Nurse P.** 1996. A quantitative model for the cdc2 control of S phase and mitosis in fission yeast. Trends Genet. **12:**345–350. http://dx.doi.org/10.1016/S0168-9525(96)80016-3.
29. **Wittenberg C, Reed SI.** 2005. Cell cycle-dependent transcription in yeast: promoters, transcription factors, and transcriptomes. Oncogene **24:** 2746–2755. http://dx.doi.org/10.1038/sj.onc.1208606.
30. **Berman J.** 2006. Morphogenesis and cell cycle progression in Candida *albicans*. Curr. Opin. Microbiol. **9:**595–601. http://dx.doi.org/10.1016/j.mib.2006.10.007.
31. **Virtudazo EV, Kawamoto S, Ohkusu M, Aoki S, Sipiczki M, Takeo K.** 2010. The single Cdk1-G_1 cyclin of *Cryptococcus neoformans* is not essential for cell cycle progression, but plays important roles in the proper commitment to DNA synthesis and bud emergence in this yeast. FEMS Yeast Res. **10:**605–618.
32. **Takeo K, Tanaka R, Miyaji M, Nishimura K.** 1995. Unbudded G_2 as well as G_1 arrest in the stationary phase of the basidiomycetous yeast *Cryptococcus neoformans*. FEMS Microbiol. Lett. **129:**231–235. http://dx.doi.org/10.1111/j.1574-6968.1995.tb07585.x.
33. **Ohkusu M, Hata K, Takeo K.** 2001. Bud emergence is gradually delayed from S to G_2 with progression of growth phase in *Cryptococcus neoformans*. FEMS Microbiol. Lett. **194:**251–255. http://dx.doi.org/10.1111/j.1574-6968.2001.tb09478.x.
34. **Neill JM, Castillo CG, Smith RH, Kapros CE.** 1949. Capsular reactions and soluble antigens of *Torula histolytica* and of *Sporotrichum schenckii*. J. Exp. Med. **89:**93–106. http://dx.doi.org/10.1084/jem.89.1.93.
35. **Mukherjee J, Cleare W, Casadevall A.** 1995. Monoclonal antibody mediated capsular reactions (Quellung) in *Cryptococcus neoformans*. J. Immunol. Methods **184:**139–143. http://dx.doi.org/10.1016/0022-1759(95)00097-T.
36. **MacGill TC, MacGill RS, Casadevall A, Kozel TR.** 2000. Biological correlates of capsular (quellung) reactions of *Cryptococcus neoformans*. J. Immunol. **164:**4835–4842. http://dx.doi.org/10.4049/jimmunol.164.9.4835.
37. **Evans EE, Garcia C, Kornfeld L, Seeliger HP.** 1956. Failure to demonstrate capsular swelling in *Cryptococcus neoformans*. Proc. Soc. Exp. Biol. Med. **93:**257–260. http://dx.doi.org/10.3181/00379727-93-22725.
38. **Cordero RJ, Bergman A, Casadevall A.** 2013. Temporal behavior of capsule enlargement by *Cryptococcus neoformans*. Eukaryot. Cell **12:** 1383–1388. http://dx.doi.org/10.1128/EC.00163-13.
39. **Castillo-Lluva S, Pérez-Martín J.** 2005. The induction of the mating program in the phytopathogen *Ustilago maydis* is controlled by a G_1 cyclin. Plant Cell **17:**3544–3560. http://dx.doi.org/10.1105/tpc.105.036319.
40. **Irniger S, Nasmyth K.** 1997. The anaphase-promoting complex is required in G_1 arrested yeast cells to inhibit B-type cyclin accumulation and to prevent uncontrolled entry into S-phase. J. Cell Sci. **110:**1523–1531.
41. **Johnston GC, Pringle JR, Hartwell LH.** 1977. Coordination of growth with cell division in the yeast *Saccharomyces cerevisiae*. Exp. Cell Res. **105:** 79–98. http://dx.doi.org/10.1016/0014-4827(77)90154-9.
42. **Hartwell LH, Unger MW.** 1977. Unequal division in *Saccharomyces cerevisiae* and its implications for the control of cell division. J. Cell Biol. **75:**422–435. http://dx.doi.org/10.1083/jcb.75.2.422.
43. **Rodrigues ML, Nakayasu ES, Oliveira DL, Nimrichter L, Nosanchuk JD, Almeida IC, Casadevall A.** 2008. Extracellular vesicles produced by *Cryptococcus neoformans* contain protein components associated with virulence. Eukaryot. Cell **7:**58–67. http://dx.doi.org/10.1128/EC.00370-07.
44. **Rodrigues ML, Nimrichter L, Oliveira DL, Frases S, Miranda K, Zaragoza O, Alvarez M, Nakouzi A, Feldmesser M, Casadevall A.** 2007. Vesicular polysaccharide export in *Cryptococcus neoformans* is a eukaryotic solution to the problem of fungal trans-cell wall transport. Eukaryot. Cell **6:**48–59. http://dx.doi.org/10.1128/EC.00318-06.
45. **Mylonakis E, Moreno R, El Khoury JB, Idnurm A, Heitman J, Calderwood SB, Ausubel FM, Diener A.** 2005. *Galleria mellonella* as a model system to study *Cryptococcus neoformans* pathogenesis. Infect. Immun. **73:**3842–3850. http://dx.doi.org/10.1128/IAI.73.7.3842-3850.2005.
46. **Zinzalla V, Graziola M, Mastriani A, Vanoni M, Alberghina L.** 2007. Rapamycin-mediated G_1 arrest involves regulation of the Cdk inhibitor Sic1 in *Saccharomyces cerevisiae*. Mol. Microbiol. **63:**1482–1494. http://dx.doi.org/10.1111/j.1365-2958.2007.05599.x.
47. **Jorgensen P, Nishikawa JL, Breitkreutz BJ, Tyers M.** 2002. Systematic identification of pathways that couple cell growth and division in yeast. Science **297:**395–400. http://dx.doi.org/10.1126/science.1070850.
48. **Hoyt MA, Totis L, Roberts BT.** 1991. *S. cerevisiae* genes required for cell cycle arrest in response to loss of microtubule function. Cell **66:**507–517. http://dx.doi.org/10.1016/0092-8674(81)90014-3.
49. **Moore SA.** 1984. Synchronous cell growth occurs upon synchronizing the two regulatory steps of the *Saccharomyces cerevisiae* cell cycle. Exp. Cell Res. **151:**542–556. http://dx.doi.org/10.1016/0014-4827(84)90402-6.
50. **Moffat J, Andrews B.** 2004. Late-G_1 cyclin-CDK activity is essential for control of cell morphogenesis in budding yeast. Nat. Cell Biol. **6:**59–66. http://dx.doi.org/10.1038/ncb1078.
51. **Lew DJ, Reed SI.** 1995. Cell cycle control of morphogenesis in budding yeast. Curr. Opin. Genet. Dev. **5:**17–23. http://dx.doi.org/10.1016/S0959-437X(95)90048-9.
52. **Lew DJ, Marini NJ, Reed SI.** 1992. Different G_1 cyclins control the timing of cell cycle commitment in mother and daughter cells of the budding yeast *S. cerevisiae*. Cell **69:**317–327. http://dx.doi.org/10.1016/0092-8674(92)90412-6.
53. **Benton BK, Tinkelenberg AH, Jean D, Plump SD, Cross FR.** 1993. Genetic analysis of Cln/Cdc28 regulation of cell morphogenesis in budding yeast. EMBO J. **12:**5267–5275.
54. **Loeb JD, Kerentseva TA, Pan T, Sepulveda-Becerra M, Liu H.** 1999. *Saccharomyces cerevisiae* G_1 cyclins are differentially involved in invasive and pseudohyphal growth independent of the filamentation mitogen-activated protein kinase pathway. Genetics **153:**1535–1546.
55. **Chapa y Lazo B, Bates S, Sudbery P.** 2005. The G_1 cyclin Cln3 regulates morphogenesis in *Candida albicans*. Eukaryot. Cell **4:**90–94. http://dx.doi.org/10.1128/EC.4.1.90-94.2005.
56. **Zaragoza O.** 2011. Multiple disguises for the same party: the concepts of morphogenesis and phenotypic variations in *Cryptococcus neoformans*. Front. Microbiol. **2:**181. http://dx.doi.org/10.3389/fmicb.2011.00181.
57. **Maxson ME, Dadachova E, Casadevall A, Zaragoza O.** 2007. Radial mass density, charge, and epitope distribution in the *Cryptococcus neoformans* capsule. Eukaryot. Cell **6:**95–109. http://dx.doi.org/10.1128/EC.00306-06.

58. **Maxson ME, Cook E, Casadevall A, Zaragoza O.** 2007. The volume and hydration of the *Cryptococcus neoformans* polysaccharide capsule. Fungal Genet. Biol. **44:**180–186. http://dx.doi.org/10.1016/j.fgb.2006.07.010.
59. **Choi YE, Goodwin SB.** 2011. Gene encoding a c-type cyclin in *Mycosphaerella graminicola* is involved in aerial mycelium formation, filamentous growth, hyphal swelling, melanin biosynthesis, stress response, and pathogenicity. Mol. Plant Microbe Interact. **24:**469–477. http://dx.doi.org/10.1094/MPMI-04-10-0090.
60. **Shim WB, Woloshuk CP.** 2001. Regulation of fumonisin B(1) biosynthesis and conidiation in *Fusarium verticillioides* by a cyclin-like (C-type) gene, FCC1. Appl. Environ. Microbiol. **67:**1607–1612. http://dx.doi.org/10.1128/AEM.67.4.1607-1612.2001.
61. **Muñoz MJ, Bejarano ER, Daga RR, Jimenez J.** 1999. The identification of Wos2, a p23 homologue that interacts with Wee1 and Cdc2 in the mitotic control of fission yeasts. Genetics **153:**1561–1572.
62. **Burnie JP, Carter TL, Hodgetts SJ, Matthews RC.** 2006. Fungal heat-shock proteins in human disease. FEMS Microbiol. Rev. **30:**53–88. http://dx.doi.org/10.1111/j.1574-6976.2005.00001.x.
63. **Zhang S, Hacham M, Panepinto J, Hu G, Shin S, Zhu X, Williamson PR.** 2006. The Hsp70 member, Ssa1, acts as a DNA-binding transcriptional co-activator of laccase in *Cryptococcus neoformans*. Mol. Microbiol. **62:**1090–1101. http://dx.doi.org/10.1111/j.1365-2958.2006.05422.x.
64. **García-Rodas R, Casadevall A, Rodríguez-Tudela JL, Cuenca-Estrella M, Zaragoza O.** 2011. *Cryptococcus neoformans* capsular enlargement and cellular gigantism during *Galleria mellonella* infection. PLoS One **6:**e24485. http://dx.doi.org/10.1371/journal.pone.0024485.
65. **Dromer F, Casadevall A, Perfect J, Sorrell T.** 2011. *Cryptococcus neoformans*: latency and disease, p 431–441. *In* Joseph Heitman TRK, Kwon-Chung KJ, Perfect JR, Casadevall A (ed), *Cryptococcus*. From human pathogen to model yeast. ASM Press, Washington, DC.
66. **Voelz K, Johnston SA, May RC.** 2011. Intracellular replication and exit strategies, p 441–451. *In* Joseph Heitman TRK, Kwon-Chung KJ, Perfect JR, Casadevall A (ed), Cryptococcus. From human pathogen to model yeast. ASM, Washington.
67. **Mcquiston T, Del Poeta M.** 2011. The interaction of *Cryptococcus neoformans* with host macrophages and neutrofils, p 373–387. *In* Joseph Heitman TRK, Kwon-Chung KJ, Perfect JR, Casadevall A (ed), Cryptococcus. From human pathogen to model host. ASM Press, Washington, DC.
68. **García-Rodas R, Zaragoza O.** 2012. Catch me if you can: phagocytosis and killing avoidance by *Cryptococcus neoformans*. FEMS Immunol. Med. Microbiol. **64:**147–161. http://dx.doi.org/10.1111/j.1574-695X.2011.00871.x.
69. **Feldmesser M, Tucker S, Casadevall A.** 2001. Intracellular parasitism of macrophages by *Cryptococcus neoformans*. Trends Microbiol. **9:**273–278. http://dx.doi.org/10.1016/S0966-842X(01)02035-2.
70. **Feldmesser M, Kress Y, Novikoff P, Casadevall A.** 2000. *Cryptococcus neoformans* is a facultative intracellular pathogen in murine pulmonary infection. Infect. Immun. **68:**4225–4237. http://dx.doi.org/10.1128/IAI.68.7.4225-4237.2000.
71. **Perfect JR, Lang SD, Durack DT.** 1980. Chronic cryptococcal meningitis: a new experimental model in rabbits. Am. J. Pathol. **101:**177–194.
72. **Raschke WC, Baird S, Ralph P, Nakoinz I.** 1978. Functional macrophage cell lines transformed by Abelson leukemia virus. Cell **15:**261–267. http://dx.doi.org/10.1016/0092-8674(78)90101-0.
73. **Mukherjee J, Casadevall A, Scharff MD.** 1993. Molecular characterization of the humoral responses to *Cryptococcus neoformans* infection and glucuronoxylomannan-tetanus toxoid conjugate immunization. J. Exp. Med. **177:**1105–1116. http://dx.doi.org/10.1084/jem.177.4.1105.
74. **Azie N, Neofytos D, Pfaller M, Meier-Kriesche HU, Quan SP, Horn D.** 2012. The PATH (Prospective Antifungal Therapy) Alliance registry and invasive fungal infections: update 2012. Diagn. Microbiol. Infect. Dis. **73:**293–300. http://dx.doi.org/10.1016/j.diagmicrobio.2012.06.012.
75. **Covert SF, Kapoor P, Lee M-H, Briley A, Nairn CJ.** 2001. *Agrobacterium tumefaciens*-mediated transformation of *Fusarium circinatum*. Mycol. Res. **105:**259–264. http://dx.doi.org/10.1017/S0953756201003872.
76. **Moyrand F, Fontaine T, Janbon G.** 2007. Systematic capsule gene disruption reveals the central role of galactose metabolism on *Cryptococcus neoformans* virulence. Mol. Microbiol. **64:**771–781. http://dx.doi.org/10.1111/j.1365-2958.2007.05695.x.
77. **Kavanagh K.** 2007. Medical mycology. Cellular and molecular techniques. Wiley, West Sussex, United Kingdom.
78. **Zaragoza O, Taborda CP, Casadevall A.** 2003. The efficacy of complement-mediated phagocytosis of *Cryptococcus neoformans* is dependent on the location of C3 in the polysaccharide capsule and involves both direct and indirect C3-mediated interactions. Eur. J. Immunol. **33:**1957–1967. http://dx.doi.org/10.1002/eji.200323848.